Polarity-Free Epitaxial Growth of Heterostructured ZnO/ZnS Core/Shell Nanobelts

ARTICLE *in* JOURNAL OF PHYSICAL CHEMISTRY LETTERS · FEBRUARY 2013

Impact Factor: 7.46 · DOI: 10.1021/jz4001533

6 AUTHORS, INCLUDING:

Xing Huang
Fritz Haber Institute of the Max Planck Society
50 PUBLICATIONS **340** CITATIONS
SEE PROFILE

Marc Georg Willinger
Fritz Haber Institute of the Max Planck Society
144 PUBLICATIONS **1,849** CITATIONS
SEE PROFILE

THE JOURNAL OF PHYSICAL CHEMISTRY Letters

Letter

pubs.acs.org/JPCL

Polarity-Free Epitaxial Growth of Heterostructured ZnO/ZnS Core/Shell Nanobelts

Xing Huang,[†,‡,⊥] Meng Wang,[†,⊥] Lidong Shao,[‡] Marc-Georg Willinger,[‡] Chun-Sing Lee,[§] and Xiang-Min Meng*[,†]

[†]Key Laboratory of Photochemical Conversion and Optoelectronic Materials, Technical Institute of Physics and Chemistry, Chinese Academy of Sciences, Beijing, 100190, People's Republic of China

[‡]Department of Inorganic Chemistry, Fritz Haber Institute of the Max Planck Society, Faradayweg 4-6, Berlin,14195, Germany

[§]Center of Super-Diamond and Advanced Films (COSDAF) and Department of Physics and Materials Science, City University of Hong Kong, Hong Kong SAR, People's Republic of China

[⊥]University of Chinese Academy of Sciences, 19A Yuquan Road, 100049 Beijing, People's Republic of China

Supporting Information

ABSTRACT: Surface-polarity-induced formation of ZnO/ZnS heterojunctions has a common characteristic that ZnS (or ZnO) is exclusively decorated on a Zn-terminated (0001) surface of ZnO (or ZnS) due to its comparatively chemically active nature to an O (or S)-terminated (000−1) surface. Here, we report a polarity-free and symmetrical growth of ZnS on both ZnO±(0001) surfaces to form a new heterostructured ZnO/ZnS core/shell nanobelt via a thermal evaporation method. Remarkably, the ZnS shell is single-crystalline and preserves the structure and orientation of the inner ZnO nanobelt with an epitaxial relationship of $(0001)_{ZnO}//(0001)_{ZnS}$; $[2-1-10]_{ZnO}//[2-1-10]_{ZnS}$. Through this case, we demonstrate that an anion-terminated polar surface could also drive the nucleation and growth of nanostructures as the cation-terminated surface by controlling the growth kinetics. Considering high-performance devices based on ZnO/ZnS heterojunctions, the current ZnO/ZnS nanobelt is advantageous for optoelectronic applications due to its single-crystalline nature and relatively more efficient charge separation along 3D heterointerfaces.

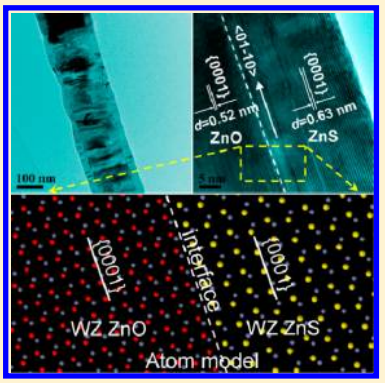

SECTION: Physical Processes in Nanomaterials and Nanostructures

One-dimensional (1D) semiconducting heterostructures are promising candidates for potential electronic and optoelectronic applications due to their integrated multifunctionality from different functional materials.[1,2] In this regard, controlled fabrication of component- and structural-modulated heterostructures at the nanoscale will be increasingly important for making devices of diverse functions.[1−4]

Being important II−VI semiconductors, ZnO and ZnS, with direct band gaps of 3.37 and 3.67 eV, respectively, are promising materials for wide applications in photocatalysis, solar cells, sensors, lasers, displays, nanogenerators, and so forth.[5−9] It has been demonstrated by both theoretical and experimental analyses that, through combining ZnO and ZnS, the heterojunction nanostructures such as core/shell nanowires,[10] biaxial nanoribbons,[11] and so forth can greatly enhance their application performances. For instance, Fang's group reported a UV-A photodetector based on the ZnO/ZnS biaxial nanobelt, which shows much higher spectral selectivity and faster response speed than those based on pure ZnS or ZnO nanostructures.[12] Considerable progress in preparing ZnO/ZnS heterstructures has been achieved by optimizing synthesis methodologies during the past decade. However, conventional synthesis commonly results in polycrystalline ZnS nanoparticles attached on the ZnO surface without a crystallographic epitaxial relationship,[13−18] thus restricting their potential applications in high-performance optoelectronics and holding back experimental support for theoretical model studies that genuinely relied on the single-crystalline nature of ZnO and ZnS with an epitaxial growth relationship.[19] Therefore, there remains an intense research interest and technical demand for fabricating structure- and orientation-regulated ZnO/ZnS heterostructures and studying in detail their growth mechanism. Recently, our study has realized an assembly of a ZnO/ZnS core/shell nanorod consisting of WZ structured ZnS epitaxially grown on the six nonpolar {01−10} planes of the ZnO nanorod.[20] Due to the lattice mismatch between ZnO and ZnS, numerous stacking faults are induced during the ZnS growth. Nevertheless, the ZnS shell is homogeneous in thickness and retains the same structure and orientation of the original ZnO.

In this work, we report a new heterostructured ZnO/ZnS core/shell nanobelt that is composed of single-crystalline WZ structured ZnS epitaxially decorated on polar ±(0001) and

Received: January 22, 2013
Accepted: February 12, 2013
Published: February 12, 2013

nonpolar ±(2−1−10) surfaces of the ZnO nanobelt. It is noteworthy that the thickness of ZnS is uniform on both polar ±(0001) planes of ZnO, which seems to be disagreed with the conventional principle and previous studies that a Zn-terminated (0001) surface is chemically active while the negatively charged O-terminated (000−1) surface is chemically inert. On the basis of the systematic characterization and analysis, the formation mechanism of this heterostructured ZnO/ZnS belt is suggested. Through this interesting phenomenon, we demonstrate that the growth behavior on the polar surface is determined not only by the surface energy but also by the growth kinetics. The synthesized ZnO/ZnS core/shell nanobelt is expected to be valuable not only for fundamental research but also for potential applications in optoelectronic devices.

The synthesis of the ZnO/ZnS core/shell nanobelt in the present work involves two processes, (i) the preparation of the ZnO nanobelt through thermal evaporation of ZnS powder with the presence of air and (ii) the growth of a ZnS shell on the prefabricated ZnO nanobelt via a second thermal deposition process. A detailed synthetic protocol of the product can be found in the Supporting Information. A scanning electron microscopy (SEM) image of the product fabricated in the first step is exhibited in Figure 1a. The displayed nanostructures are about several to several tens of micrometers long and 40−350 nm in diameter. It is found that the product is composed of up to 40% of nanobelts in addition to the wire-like nanostructures. An energy-dispersive X-ray spectroscopy (EDX) study (Figure S1a, Supporting Information) of the product shows the existence of only Zn and O elements without detectable impurity. X-ray diffraction (XRD) analysis (Figure S1b, Supporting Information) further confirms that it contains a single phase of WZ structured ZnO with lattice constants a = 0.3249 and c = 0.5206 nm (JCPDS: 36-1451). Transmission electron microscopy (TEM) was then employed to investigate the detailed morphology and structure of the as-prepared ZnO nanostructures. A typical TEM image of a single ZnO nanobelt is given in Figure 1b. As can be seen, the well-defined nanobelt with smooth side surfaces is about 120 nm in width. The corresponding selected area electron diffraction (SAED) pattern (inset of Figure 1b) and high-resolution TEM (HRTEM) image (Figure 1c) indicate that the as-prepared ZnO nanobelt, with its top/down surfaces of ±(2−1−10) and side surfaces of ±(0001), is single-crystalline and grows along the <01−10> direction of the WZ structure.

Using the prepared ZnO nanobelts as templates and ZnS powder as the source material, a second deposition process was carried out. Figure 2a shows a representative TEM image of the nanobelt obtained after the reaction. The bright/dark contrast variation along the radial direction can be clearly observed, indicating a core/shell configuration of the heterostructured nanobelt. The SAED pattern (Figure 2b) shows two well-aligned sets of rectangular spots, which can be respectively indexed as the WZ structured ZnO and ZnS. Shown in Figure 2c is a HRTEM image of the nanobelt. Two sets of epitaxially aligned lattice fringes of 0.52 and 0.63 nm at the core and shell regions match well to {0001} planes of WZ ZnO and ZnS, respectively. Such an epitaxial characteristic is schematically illustrated with an atomic model (Figure 2d), and the epitaxial relationship between ZnO and ZnS is $(0001)_{ZnO}//(0001)_{ZnS}$; $[2-1-10]_{ZnO}//[2-1-10]_{ZnS}$. Compared with the core/shell nanowire with heterointerfaces of {01−10} planes (Figure S2, Supporting Information), the ZnS shell on ZnO {0001} planes

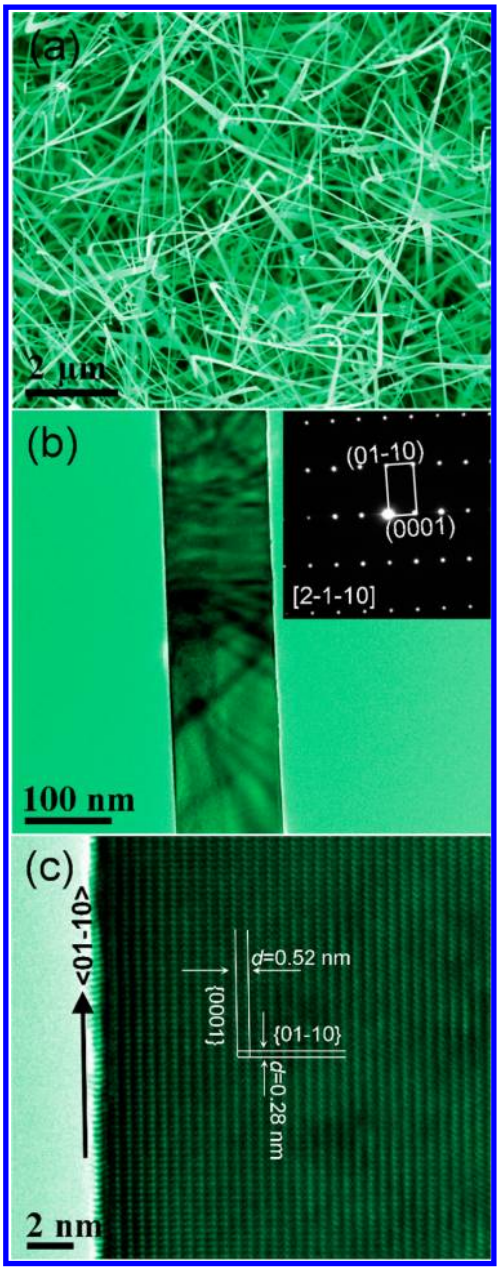

Figure 1. (a) SEM image the synthesized ZnO nanostructures. (b) TEM and (c) HRTEM image of a single ZnO nanobelt; the inset of (b) is the corresponding SAED pattern of the ZnO nanobelt.

of the current core/shell nanobelt exhibits much fewer structural defects due to the less lattice mismatch of {01−10} than {0001} planes between ZnO and ZnS. A detailed compositional analysis of the nanobelt was further performed using EDX in a scanning TEM (STEM). Panels e and f–h of Figure 2 show a high-angle annular dark field (HAADF) image and STEM-EDX elemental mapping of a nanobelt, respectively. It can be vividly seen that the O elements are concentrated only at the core region while the Zn and S signals disperse at the entire nanobelt, which again confirms the core/shell configuration of the as-obtained ZnO/ZnS nanobelt. Considering the high performance of the ZnO/ZnS biaxial nanobelt as a UV-A detector arising from the charge separation of type-II band alignment along the 1D heterointerface,[12] our architecture here may present even higher optoelectronic properties due not only to its single-crystalline feature but also to the efficient spatial

dx.doi.org/10.1021/jz4001533 | J. Phys. Chem. Lett. 2013, 4, 740−744

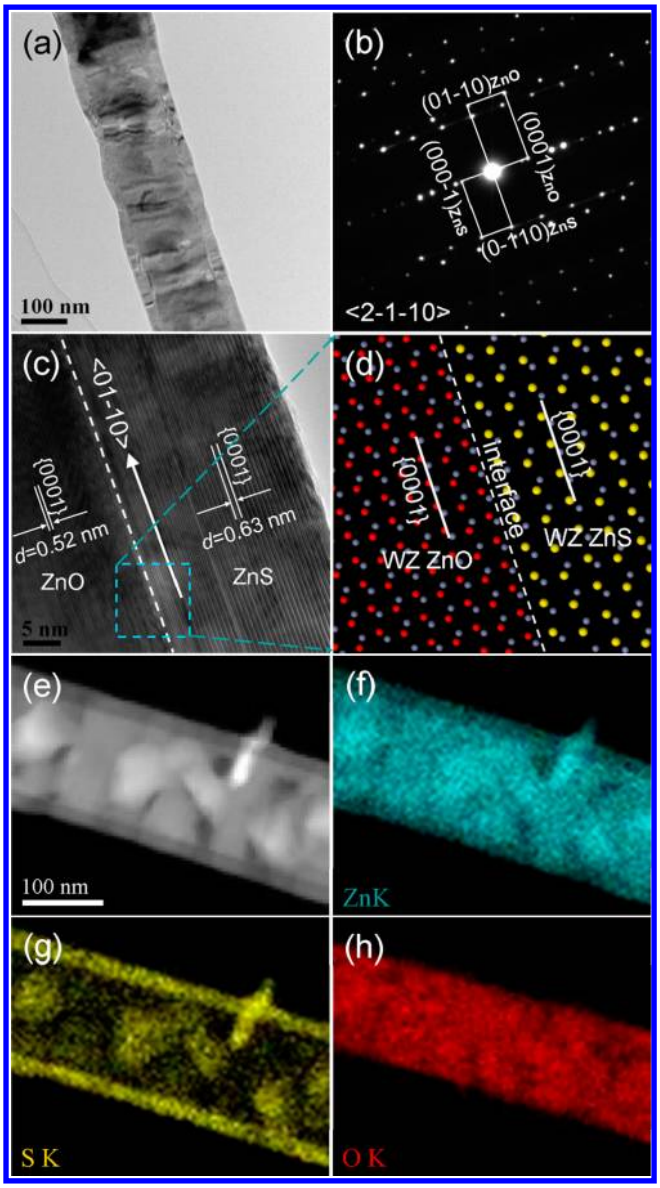

Figure 2. (a) TEM image, (b) corresponding SAED pattern, (c) HRTEM image, (d) atom model, (e) HAADF image, and (f–h) STEM-EDX elemental mapping of the ZnO/ZnS core/shell nanobelt.

charge separation along the 3D heterointerfaces between ZnO and ZnS. Further investigation will be carried out.

ZnO, known as the most representative WZ structured material, structurally, can be described schematically as a number of alternating planes of tetrahedrally coordinated O^{2-} and Zn^{2+} ions stacked alternatively along the *c* axis.[21−23] The oppositely charged ions produce positively charged Zn−(0001) and negatively charged O−(000−1) polar surfaces. It is generally believed that the Zn-terminated (0001) surface is chemically active, while the negatively charged O-terminated (000−1) surface is relatively chemically inert.[22,24] The formation of ZnO nanostructures induced by polar charge and self-catalysis of the cation-terminated surface has been reported in a variety of morphologies, such as nanospirals,[21] nanohelixes,[23] nanorings,[25] nanocombs,[26] and so forth. In the case of ZnO/ZnS heterojunctions, Wang's group has presented a new ring structure that is composed of ZnS exclusively decorated on the Zn-terminated (0001) surface of ZnO.[22] A similar result has been demonstrated as well by Yang et al. that the ZnO nanowire only grows on the Zn−(0001) plane of the ZnS nanobelt to form a ZnO nanowire/ZnS nanobelt heterostructure.[24] However, in the present work, the ZnO nanobelt has been fully decorated with a layer of single-crystalline ZnS, and especially, the thickness of ZnS along the two polar ±(0001) planes of ZnO is almost the same, as shown in Figure 2a and e. This polarity-free and symmetrical growth indicates that through controlling the growth kinetics, the anion-terminated polar surface can also facilitate the nucleation and growth of nanostructures equal to the cation-terminated surface. This result may give some guidance for rationally designing other heterostructures that involves the heterogrowth behaviors on the polar surfaces.

On the basis of our previous study and the above analysis, the formation of a single-crystalline ZnO/ZnS core/shell nanobelt can be explained as following: first, the constant heating of ZnO nanostructures at 600 °C in the deposition area activates both the Zn^{2+} and O^{2-} ions of ZnO on the surface, and then, they react with the H_2S generated by a hydrogen-assisted thermal evaporation process to form a thin initial ZnS on the surface of the ZnO nanobelt.[27] This reaction essentially is a substitution reaction, that is, O^{2-} of ZnO is substituted for S^{2-};[16,28] thus, the formed ZnS layer preserves the single-crystalline characteristic and crystallographic orientation of the original ZnO nanobelt.[29] After that, the formed ZnS layer would limit the further proceeding of the substitution reaction and then serve as a substrate for the nucleation and epitaxial growth on ±(0001) and ±(2−1−10) surfaces of ZnS. The whole process is schematically illustrated in Figure 3. With these reactions, the

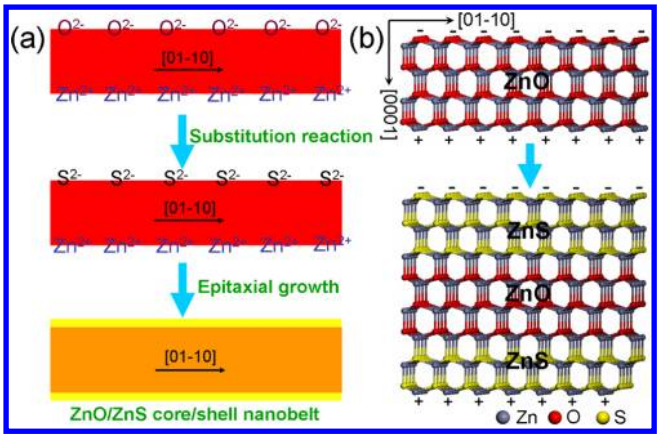

Figure 3. (a) Schematic growth process of the ZnO/ZnS core/shell nanobelt;. (b) Atom models of the ZnO and the ZnO/ZnS core/shell nanobelt.

single-crystalline WZ structured ZnS shell epitaxially grew on the ZnO nanobelt to form a heterostructured ZnO/ZnS core/shell nanobelt eventually. In this work, the temperature of the deposition area is a key factor to determine whether the ZnS shell can grow on the ZnO nanobelt during the coating process. It was found that when the temperature was lower than 500 °C, the core/shell heterostructures could be rarely formed. This is probably because the external ZnO has not been activated yet at that temperature and thereby disables the further proceeding of the substitution reaction and the followed epitaxial growth of ZnS.

Over the past decade, tubular ZnS nanostructures have been extensively studied owing to their potential uses in electronics

dx.doi.org/10.1021/jz4001533 | J. Phys. Chem. Lett. 2013, 4, 740−744

and optoelectronics. However, the previously reported ZnS nanotubes are generally composed of numerous polycrystalline nanocrystallites,[13,16,17,30−32] which would affect their performance in electronic and optoelectronic applications.[33] To date, it remains challenging for a rational synthesis of single-crystalline WZ structured ZnS nanotubes. In the present work, upon removing the inner ZnO cores through a solution process, ZnS hollow nanotubes can be simply prepared. Figure 4a shows a

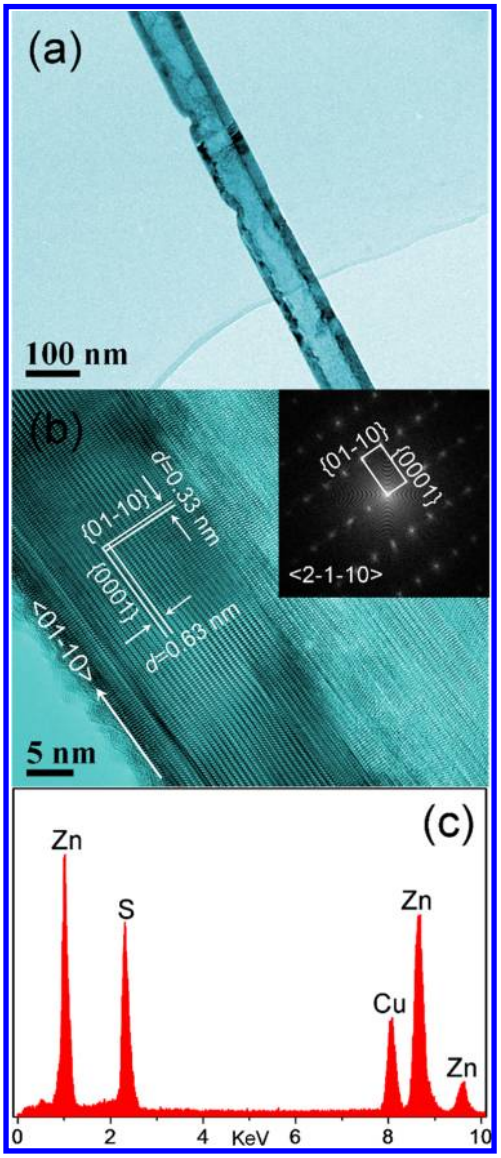

Figure 4. (a) TEM image and (b) HRTEM image as well as its corresponding FFT pattern of the ZnS nanotube. (c) EDX data of the ZnS nanotube.

representative TEM image of the product after an acetic acid solution treatment, from which a hollow construction of the ZnS nanotube can be revealed. EDX analysis (Figure 4c) shows only Zn and S elements, indicating a complete dissolution and removal of the inner ZnO cores. The HRTEM image and the fast Fourier transform (FFT) pattern were also taken (Figure 4b), which demonstrate that the ZnS tube is single-crystalline and has a growth direction of <01−10>, in accordance to the previous observation. As far as we know, this is the first time that rectangular ZnS nanotubes with a WZ structure were achieved in single-crystalline form. Thus, our work as well can be demonstrated as a simple route for a rational realization of well-crystallized ZnS hollow nanotubes, which are considered as highly promising candidates for novel electronic and optoelectronic applications due to their high surface area and single-crystalline nature.[9,33]

In summary, we have presented a new heterostructured ZnO/ZnS core/shell nanobelt in this work. The ZnS shell epitaxially grows on the entire ZnO nanobelt with an orientation relationship of $(0001)_{ZnO}//(0001)_{ZnS}$; $[2{-}1{-}10]_{ZnO}//[2{-}1{-}10]_{ZnS}$. In particular, the polarity-free and symmetrical growth of ZnS on the ZnO±(0001) surfaces has been demonstrated in the current system, which reveals that growth behavior on the polar surfaces can be tailored through the growth kinetics control. After removal of the ZnO core, a single-crystalline rectangular ZnS nanotube defined by polar {0001} and nonpolar {2−1−10} surfaces has been obtained with an axial direction of <01−10> for the first time. The formation process of the core/shell nanobelt has been proposed to involve a substitution reaction followed by an epitaxial growth of ZnS. The heterostructured ZnO/ZnS core/shell nanobelt and ZnS hollow nanotube provide ideal candidates for studying and optimizing the optoelectronic performances of II−VI semiconductors.

■ ASSOCIATED CONTENT

Supporting Information

Detailed synthetic protocol of the product; experimental techniques employed; EDX and XRD spectra of the ZnO nanostructures; TEM, HRTEM, corresponding atom model, HAADF image, and STEM-EDX mapping of the ZnO/ZnS core/shell nanowire. This material is available free of charge via the Internet at http://pubs.acs.org.

■ AUTHOR INFORMATION

Corresponding Author

*E-mail: mengxiangmin@mail.ipc.ac.cn.

Notes

The authors declare no competing financial interest.

■ ACKNOWLEDGMENTS

We would like to acknowledge the financial support from the National Natural Science Foundation of China (21073212) and the 973 Project (2009CB623003).

■ REFERENCES

(1) Lauhon, L. J.; Gudiksen, M. S.; Wang, C. L.; Lieber, C. M. Epitaxial Core−Shell and Core−Multishell Nanowire Heterostructures. *Nature* **2002**, *420*, 57−61.

(2) Shen, S.; Zhang, Y.; Peng, L.; Du, Y.; Wang, Q. Matchstick-Shaped Ag_2S−ZnS Heteronanostructures Preserving Both UV/Blue and Near-Infrared Photoluminescence. *Angew. Chem., Int. Ed.* **2011**, *50*, 7115−7118.

(3) Chuang, C.-H.; Lo, S. S.; Scholes, G. D.; Burda, C. Charge Separation and Recombination in CdTe/CdSe Core/Shell Nanocrystals As a Function of Shell Coverage: Probing the Onset of the Quasi Type-II Regime. *J. Phys. Chem. Lett.* **2010**, *1*, 2530−2535.

(4) Myung, Y.; Jang, D. M.; Sung, T. K.; Sohn, Y. J.; Jung, G. B.; Cho, Y. J.; Kim, H. S.; Park, J. Composition-Tuned ZnO−CdSSe Core−Shell Nanowire Arrays. *ACS Nano* **2010**, *4*, 3789−3800.

(5) Wang, Z. L. ZnO Nanowire and Nanobelt Platform for Nanotechnology. *Mater. Sci. Eng. R.* **2009**, *64*, 33−71.

(6) Lee, J.; Shim, H. S.; Lee, M.; Song, J. K.; Lee, D. Size-Controlled Electron Transfer and Photocatalytic Activity of ZnO−Au Nanoparticle Composites. *J. Phys. Chem. Lett.* **2011**, *2*, 2840−2845.
(7) Wang, Z. L.; Song, J. H. Piezoelectric Nanogenerators Based on Zinc Oxide Nanowire Arrays. *Science* **2006**, *312*, 242−246.
(8) Fang, X.; Bando, Y.; Liao, M.; Zhai, T.; Gautam, U. K.; Li, L.; Koide, Y.; Golberg, D. An Efficient Way to Assemble ZnS Nanobelts as Ultraviolet-Light Sensors with Enhanced Photocurrent and Stability. *Adv. Funct. Mater.* **2010**, *20*, 500−508.
(9) Fang, X.; Wu, L.; Hu, L. ZnS Nanostructure Arrays: A Developing Material Star. *Adv. Mater.* **2011**, *23*, 585−598.
(10) Wang, K.; Chen, J. J.; Zeng, Z. M.; Tarr, J.; Zhou, W. L.; Zhang, Y.; Yan, Y. F.; Jiang, C. S.; Pern, J.; Mascarenhas, A. Synthesis and Photovoltaic Effect of Vertically Aligned ZnO/ZnS Core/Shell Nanowire Arrays. *Appl. Phys. Lett.* **2010**, *96*, 123105.
(11) Yan, J.; Fang, X.; Zhang, L.; Bando, Y.; Gautam, U. K.; Dierre, B.; Sekiguchi, T.; Golberg, D. Structure and Cathodoluminescence of Individual ZnS/ZnO Biaxial Nanobelt Heterostructures. *Nano Lett.* **2008**, *8*, 2794−2799.
(12) Hu, L.; Yan, J.; Liao, M.; Xiang, H.; Gong, X.; Zhang, L.; Fang, X. An Optimized Ultraviolet-A Light Photodetector with Wide-Range Photoresponse Based on ZnS/ZnO Biaxial Nanobelt. *Adv. Mater.* **2012**, *24*, 2305−2309.
(13) Yan, C.; Xue, D. Conversion of ZnO Nanorod Arrays into ZnO/ZnS Nanocable and ZnS Nanotube Arrays via an In Situ Chemistry Strategy. *J. Phys. Chem. B* **2006**, *110*, 25850−25855.
(14) Hu, Y.; Qian, H.; Liu, Y.; Du, G.; Zhang, F.; Wang, L.; Hu, X. A Microwave-Assisted Rapid Route to Synthesize ZnO/ZnS Core−Shell Nanostructures via Controllable Surface Sulfidation of ZnO Nanorods. *CrystEngComm* **2011**, *13*, 3438−3443.
(15) Lin, D.; Wu, H.; Zhang, R.; Zhang, W.; Pan, W. Facile Synthesis of Heterostructured ZnO−ZnS Nanocables and Enhanced Photocatalytic Activity. *J. Am. Ceram. Soc.* **2010**, *93*, 3384−3389.
(16) Wang, X. D.; Gao, P. X.; Li, J.; Summers, C. J.; Wang, Z. L. Rectangular Porous ZnO−ZnS Nanocables and ZnS Nanotubes. *Adv. Mater.* **2002**, *14*, 1732−1735.
(17) Wang, Z.; Qian, X. F.; Li, Y.; Yin, J.; Zhu, Z. K. Large-Scale Synthesis of Tube-Like ZnS and Cable-Like ZnS−ZnO Arrays: Preparation Through the Sulfuration Conversion from ZnO Arrays via a Simple Chemical Solution Route. *J. Solid State Chem.* **2005**, *178*, 1589−1594.
(18) Bera, A.; Basak, D. Photoluminescence and Photoconductivity of ZnS-Coated ZnO Nanowires. *ACS Appl. Mater. Interfaces* **2010**, *2*, 408−412.
(19) Schrier, J.; Demchenko, D. O.; Wang, L.-W. Optical Properties of ZnO/ZnS and ZnO/ZnTe Heterostructures for Photovoltaic Applications. *Nano Lett.* **2007**, *7*, 2377−2382.
(20) Huang, X.; Wang, M.; Willinger, M.-G.; Shao, L.; Su, D. S.; Meng, X.-M. Assembly of Three-Dimensional Hetero-Epitaxial ZnO/ZnS Core/Shell Nanorod and Single Crystalline Hollow ZnS Nanotube Arrays. *ACS Nano* **2012**, *6*, 7333−7339.
(21) Kong, X. Y.; Wang, Z. L. Polar-Surface Dominated ZnO Nanobelts and the Electrostatic Energy Induced Nanohelixes, Nanosprings, and Nanospirals. *Appl. Phys. Lett.* **2004**, *84*, 975−977.
(22) Wu, X.; Jiang, P.; Ding, Y.; Cai, W.; Xie, S.-S.; Wang, Z. L. Mismatch Strain Induced Formation of ZnO/ZnS Heterostructured Rings. *Adv. Mater.* **2007**, *19*, 2319−2323.
(23) Gao, P. X.; Ding, Y.; Mai, W. J.; Hughes, W. L.; Lao, C. S.; Wang, Z. L. Conversion of Zinc Oxide Nanobelts into Superlattice-Structured Nanohelices. *Science* **2005**, *309*, 1700−1704.
(24) Wang, Z.; Liu, X.; Gong, J.; Huang, H.; Gu, S.; Yang, S. Epitaxial Growth of ZnO Nanowires on ZnS Nanobelts by Metal Organic Chemical Vapor Deposition. *Cryst. Growth Des.* **2008**, *8*, 3911−3913.
(25) Kong, X. Y.; Ding, Y.; Yang, R.; Wang, Z. L. Single-Crystal Nanorings Formed by Epitaxial Self-Coiling of Polar Nanobelts. *Science* **2004**, *303*, 1348−1351.
(26) Wang, Z. L.; Kong, X. Y.; Zuo, J. M. Induced Growth of Asymmetric Nanocantilever Arrays on Polar Surfaces. *Phys. Rev. Lett.* **2003**, *91*, 185502.
(27) Jiang, Y.; Meng, X. M.; Liu, J.; Xie, Z. Y.; Lee, C. S.; Lee, S. T. Hydrogen-Assisted Thermal Evaporation Synthesis of ZnS Nanoribbons on a Large Scale. *Adv. Mater.* **2003**, *15*, 323−327.
(28) Panda, S. K.; Dev, A.; Chaudhuri, S. Fabrication and Luminescent Properties of *c*-Axis Oriented ZnO−ZnS Core−Shell and ZnS Nanorod Arrays by Sulfidation of Aligned ZnO Nanorod Arrays. *J. Phys. Chem. C* **2007**, *111*, 5039−5043.
(29) Park, J.; Zheng, H.; Jun, Y.-W.; Alivisatos, A. P. Hetero-Epitaxial Anion Exchange Yields Single-Crystalline Hollow Nanoparticles. *J. Am. Chem. Soc.* **2009**, *131*, 13943−13945.
(30) Zhai, T.; Gu, Z.; Ma, Y.; Yang, W.; Zhao, L.; Yao, J. Synthesis of Ordered ZnS Nanotubes by MOCVD-Template Method. *Mater. Chem. Phys.* **2006**, *100*, 281−284.
(31) Yi, R.; Qiu, G.; Liu, X. Rational Synthetic Strategy: From ZnO Nanorods to ZnS Nanotubes. *J. Solid State Chem.* **2009**, *182*, 2791−2795.
(32) Lv, R. T.; Cao, C. B.; Guo, Y. J.; Zhu, H. S. Preparation of ZnS Nanotubes via Surfactant Micelle-Template Inducing Reaction. *J. Mater. Sci.* **2004**, *39*, 1575−1578.
(33) Yin, L. W.; Bando, Y.; Zhan, J. H.; Li, M. S.; Golberg, D. Self-Assembled Highly Faceted Wurtzite-Type ZnS Single-Crystalline Nanotubes with Hexagonal Cross-Sections. *Adv. Mater.* **2005**, *17*, 1972−1977.